Single-crystal neutron diffraction and Mössbauer spectroscopic study of hureaulite, $(Mn,Fe)_5(PO_4)_2(HPO_4)_2(H_2O)_4$

G. Diego Gatta[1,2,*], Günther J. Redhammer[3], Pietro Vignola[1,4], Martin Meven[5] and Garry J. McIntyre[6]

[1] Dipartimento di Scienze della Terra, Università degli Studi di Milano, Via Botticelli 23, 20133 Milano, Italy

[2] CNR - Istituto di Cristallografia, Via G. Amendola 122/o, Bari, Italy

*Corresponding author, e-mail: diego.gatta@unimi.it

[3] Abteilung für Mineralogie, FB Materialforschung & Physik, Universität Salzburg, Hellbrunnerstr. 34/III, 5020 Salzburg, Austria

[4] CNR-Istituto per la Dinamica dei Processi Ambientali, Milano, Italy

[5] Institut für Kristallographie, RWTH Aachen, and Jülich Centre for Neutron Science (JCNS), Forschungszentrum Jülich GmbH, at Heinz Maier-Leibnitz Zentrum (MLZ), Lichtenbergstasse 1, 85748 Garching, Germany

[6] Australian Nuclear Science and Technology Organization, Locked Bag 2001, Kirrawee DC NSW 2232, Australia

Abstract: The crystal chemistry of hureaulite from the Jocão (Cigana) pegmatite, Conselheiro Pena, Doce Valley, Minas Gerais (Brazil), was investigated by electron microprobe analysis in wavelength-dispersive mode, single-crystal Laue (at 293 K) and monochromatic neutron diffraction (at 2.3 K), and ^{57}Fe-Mössbauer spectroscopy [$^{M(1),M(2),M(3)}(Mn^{2+}_{3.61}Fe^{2+}_{1.21}Ca_{0.11}Mg_{0.03})_{\sum=4.96}(^{P(2)}PO_4)_2$ $(H_{1.04}{}^{P(1)}PO_4)_2(H_2O)_{3.92}$, $Z = 4$, $a = 17.603(6)$, $b = 9.087(2)$, $c = 9.404(4)$ Å, $\beta = 96.66(4)°$, and $V = 1494.1(9)$ Å^3 at 293 K, space group $C2/c$]. The neutron refinements confirm the general structure model previously reported, showing that five independent H sites (with full site occupancy) occur in the hureaulite structure, one of them as member of the unique hydroxyl group (*i.e.*, $O(1)$-$H(1)$) and the other four belonging to two independent H_2O molecules (*i.e.*, $H(2)$-$O(9)$-$H(3)$ and $H(4)$-$O(10)$-$H(5)$). The hydroxyl group is the vertex of one of the two independent P-tetrahedra (*i.e.*, $HOPO_3$), whereas the two H_2O molecules are the vertices of the (Mn,Fe)-octahedra. No zeolitic H_2O occurs in hureaulite structure. The complex hydrogen bonding scheme in hureaulite is now well defined, with five hydrogen bonds energetically favorable. The element distribution among the octahedral sites, deduced on the basis of the neutron structure refinements, shows that the highest fraction of Fe populates the *M(2)* site (~36%), whereas lower fractions are observed at *M(1)* and *M(3)* (*i.e.*, ~13–15 and ~11–12%, respectively). The ^{57}Fe Mössbauer spectrum of hureaulite confirms the absence of ferric iron in the sample. The spectrum shows four well-separated absorption lines which are best fitted with three doublets. The well-resolved doublet (with the largest quadrupole splitting) is here assigned to the *M(3)* site, in line with the pronounced preference of Mn^{2+} for the *M(3)* site as shown by the neutron structure refinements. The two innermost doublets have almost identical isomer shifts, though with slightly different quadrupole splitting values; the smaller quadrupole splitting value is assigned to the *M(2)* site, which is expected to have a slightly lower polyhedral distortion than the *M(1)* site, according to the experimental findings based on the neutron refinements.

Key-words: hureaulite; electron microprobe analysis (WDS); single-crystal neutron diffraction; Mössbauer spectroscopy; hydrogen bonding; phosphate.

Introduction

Phosphate minerals represent the major host of transition metals and H_2O in quartzofeldspathic pegmatitic rocks. Iron-manganese phosphate minerals are widespread in medium-to-highly-evolved granitic pegmatites, ranging from the beryl–columbite–phosphate subtype to the spodumene subtype. These phosphates play an essential geochemical role in the evolution processes affecting pegmatites, and a good knowledge of their crystal chemistry and of their stability fields is necessary to understand better the genesis of pegmatites and the medium- to low-temperature crystallization processes. We have recently contributed to exploration of the labyrinthine world of hydrous transition-metal phosphates with a series of studies, mainly based on single-crystal neutron diffraction, in order to locate clearly H and to distinguish the structural roles of atoms of similar atomic number, such as Mn and Fe (*e.g.*, Gatta *et al.*, 2013a, 2013b, 2014a, 2014b; Vignola *et al.*, 2014). We have extended our investigation to a further member of the phosphate minerals group: hureaulite. Hureaulite, ideally $(Mn,Fe)_5(PO_4)_2(HPO_4)_2(H_2O)_4$, was discovered in 1825 by the ceramicist François Alluaud II (Vauquelin, 1825; Alluaud, 1826) in the pegmatite quarry of Hureaux (from which its name originates) in Haute
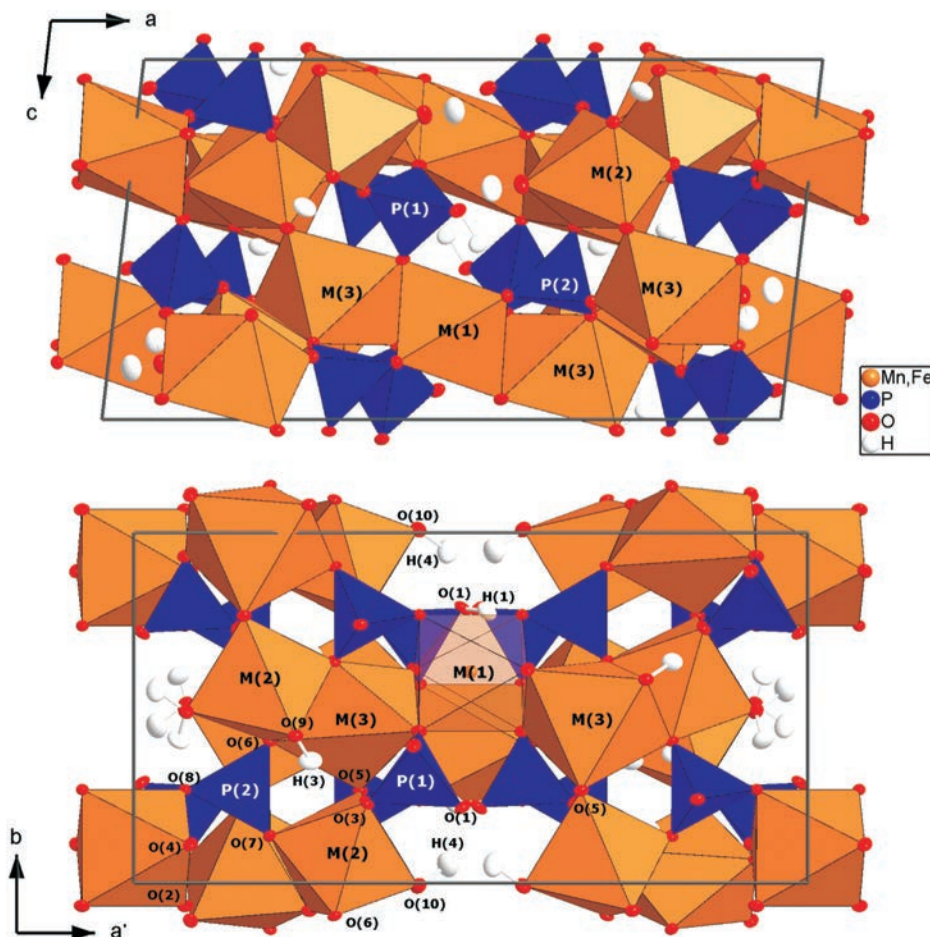
Fig. 1. Two views of the crystal structure of hureaulite based on the neutron structure refinement (at 293 K) of this study. Displacement ellipsoid probability factor: 50%. (online version in colour)

Vienne, France. It is a widespread, late-stage secondary phosphate mineral formed by alteration of primary phosphates, mainly lithiophilite ($LiMn^{2+}PO_4$), in strongly differentiated lithium–caesium–tantalum (LCT) granite pegmatites (Fransolet, 1976; Huminicki & Hawthorne, 2002), spanning from the beryl–columbite–phosphate to the lepidolite subtype, according to the classification of Černý & Ercit (2005). Hureaulite is expected to crystallize during the hydrothermal stage in non-oxidizing conditions between 300 and 100°C (*e.g.* Simmons *et al.*, 2003). The petrogenetic process leading to the formation of hureaulite after lithiophilite occurs mainly in strongly Ta- and Li-enriched pegmatites, which are extremely interesting from the economic point of view, being, with carbonatites, one of the two natural sources of the strategic elements Ta and Nb.

The knowledge of the crystal chemistry of hureaulite is restricted to a few studies, with some conflicting results. Fisher (1964) first described this mineral as monoclinic (space group *C*2/*c*) with $a \sim 17.59$, $b \sim 9.08$, $c \sim 9.40$ Å, and $\beta \sim 96.7°$ ($Z = 4$), providing the chemical analyses of samples from different localities. The crystal structure of hureaulite was solved and refined independently by Menchetti & Sabelli (1973) and Moore & Araki (1973),

confirming the space group and the metrics reported by Fisher (1964). The structure consists of PO_4 and $HOPO_3$ tetrahedra (Fig. 1), linked together by groups of edge-sharing Mn octahedra (and by hydrogen bonds) (Fig. 1). All H_2O molecules in hureaulite appeared to be bonded to the transition metals, behaving as ligand groups. Moore & Araki (1973) did not provide any H positions, and only isotropic displacement parameters of all the other atomic sites were given. Menchetti & Sabelli (1973) provided a partially anisotropic refinement, listing also the potential coordinates of the H sites (in five independent sites), which were fixed but not refined. The structure models of hureaulite of Moore & Araki (1973) and Manchetti & Sabelli (1973) are mutually consistent and agree with the experimental findings of Gerault *et al.* (1987) on the synthetic $Mn_5(HPO_4)_2(PO_4)_2(H_2O)_4$. Keller (1971) reported for hureaulite three possible crystal-chemical formulae: i) $(Mn,Fe)_5(H_3O)_2(PO_4)_4 \cdot 2H_2O$; ii) $(Mn,Fe)_5[(OH)_2(HOPO_3)_4]\cdot 2H_2O$; iii) $(Mn,Fe)_5[(HOPO_3)_2(PO_4)_2]\cdot 4H_2O$. The infrared study of Keller (1971) showed no clear evidence of the presence of $HOPO_3^{2-}$ groups, but suggested the presence of the H_3O^+ ion. A more recent infrared study on a polycrystalline sample of hureaulite was reported by Frost & Erickson (2005); however, the sample was not well

characterized (*i.e.*, no chemical or crystallographic data were provided) and only a general assignment of the active bands was reported, without any crystallographic implication.

A few Mössbauer studies on hureaulite-type materials have so far been published, the first dates back to Moreira *et al.* (1994), who investigated nine synthetic samples across a complete solid-solution series $(Fe_xMn_{5-x})(PO_4H)_2(PO_4)_2(H_2O)_4$, determining the site occupation and range of hyperfine parameters. For the pure end-member composition (*i.e.*, x = 5) they assigned the doublet with the lowest area fraction to the *M(1)* site, in accordance with the site occupation ratio of 1:2:2 for *M(1)*:*M(2)*:*M(3)*. This lowest-intensity doublet had, on the other hand, the smallest quadrupole splitting. Conversely, the doublet with the largest quadrupole splitting was ascribed to the *M(3)* site, which has the most distorted oxygen-atom environment of all the three sites. From changes in site occupation numbers of Fe^{2+} across the solid solution, Moreira *et al.* (1994) found that Mn^{2+} preferentially populates the most distorted *M(3)* site. Later on, Bustamente *et al.* (2005) reinvestigated the Mössbauer spectrum of the synthetic ferrous end-member; they used the site assignment proposed by Moreira *et al.* (1994), giving supporting arguments for it from calculation of polyhedral distortion parameters derived from single-crystal X-ray diffraction on the material. Dyar *et al.* (2014) compiled a large number of Mössbauer data for iron phosphates, including hureaulite, which contains Fe^{2+} only in two positions, namely the *M(2)* and the *M(3)* ones.

We recovered nearly transparent, pink crystals of hureaulite from the strongly evolved and Ta/Li-bearing pegmatitic dykes outcropping near the village of Conselheiro Pena (Minas Gerais, Brazil), suitable for single-crystal neutron diffraction investigation. In this light, the aim of the present study is a reinvestigation of the crystal structure and crystal chemistry of a natural hureaulite by means of electron-microprobe analysis in wavelength-dispersive mode (EPMA-WDS), Mössbauer spectroscopy (on a polycrystalline sample) and single-crystal neutron diffraction in order to provide: *a)* the reliable location of the proton sites, their anisotropic displacement parameters and the real topological configuration of the OH groups and H_2O molecules, with a full description of the H-bond network; *b)* the Mn/Fe ordering between the octahedral sites; *c)* the oxidation state and the local coordination environment of Mn and Fe.

Sample description and mineralogy

Pale pink, transparent, millimetric crystals of hureaulite from the private collection of one of the authors (P.V., catalogue #3021), coming from the Jocão (Cigana) pegmatite, Conselheiro Pena, Doce Valley, Minas Gerais, Brazil, were used for this multi-methodological study.

The Jocão pegmatite, located on the east side of the Rio Doce river and close to the town of Galiléia, belongs to the Eastern Brazilian Pegmatite Province and is hosted by high-grade mica schists of the Sao Tomé formation (Pedrosa-Soares *et al.*, 2009). This strongly fractionated

pegmatitic dyke, belonging to the beryl–columbite–phosphates subtype in the classification of Černý & Ercit (2005), shows a rather simple primary phosphate association given by triphylite + beusite (*e.g.* Baijot *et al.*, 2014). According to Baijot *et al.* (2014), three different primary phosphate associations originate several secondary phosphate assemblages containing hureaulite as a common product of alteration. The three primary phosphate associations originate three kinds of hureaulite, which are different both in the aspect and chemical composition. The specimen of hureaulite used in this study corresponds to the ''hureaulite II'' described by Baijot *et al.* (2014). A description of other associated minerals at the Jocão (Cigana) pegmatite, among which the recently discovered correianevesite, is given in Chukanov *et al.* (2014).

Experimental methods

1) Chemical analysis

The chemical composition of the hureaulite from Jocão was investigated by EPMA-WDS. After a preliminary EDS investigation, quantitative EPMA-WDS analyses were performed on a polished and carbon-coated fragment of a crystal of approximately $2 \times 2 \times 2$ mm^3, optically free of defects, using a Jeol JXA-8200 electron microprobe. The system was operated using a defocused electron beam (Ø 5 μm), an accelerating voltage of 15 kV, a beam current of 5 nA measured by a Faraday cup and counting time of 30 s on peaks and 10 s on backgrounds. Natural crystals of graftonite (for P, Fe, Mn and Ca), forsterite (for Mg), and rhodonite (for Zn) were used as standards. The results were corrected for matrix effects using a conventional φρZ routine as implemented in the JEOL suite of programs. The crystal was found to be chemically homogeneous within the analytical error, though with several micro-fractures. The chemical formula, obtained by averaging seven point analyses, is given in Table 1.

2) Single-crystal X-ray and neutron diffraction experiments

Single crystals of hureaulite, optically free of inclusions under a transmitted-light polarizing microscope, were selected for the diffraction experiments. The unit-cell parameters at 293 K were first measured by single-crystal X-ray diffraction (using a small crystal with dimensions $0.215 \times 0.130 \times 0.08$ mm^3) with a KUMA four-circle diffractometer equipped with a point detector. A total of 38 reflections were centred giving a metrically monoclinic unit-cell with: $a = 17.603(6)$, $b = 9.087(2)$, $c = 9.404(4)$ Å, $\beta = 96.66(4)°$, and $V = 1494.1(9)$ Å^3 (Table 2).
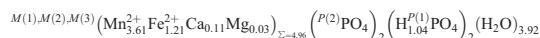
A series of crystals were selected for the polychromatic (at 293 K) and monochromatic (at 2.3 K) neutron diffraction experiments. However, the diffraction patterns showed that all the crystals of the hureaulite sample (used in this study) larger than 1 mm^3 were severely affected by

Table 1. Representative composition of the hureaulite from Jocão (Cigana) pegmatite, based on EPMA-WDS analysis (average of 7 data points).

	wt%	e.s.d.		a.p.f.u.[§]
P_2O_5	39.20	0.50	P	4.00
FeO	12.03	0.16	Fe^{2+}	1.21
MnO	35.38	0.71	Mn^{2+}	3.61
MgO	0.15	0.04	Mg	0.03
ZnO	0.04	0.03	Zn	< 0.01
CaO	0.85	0.08	Ca	0.11
H_2O*	12.35		H	9.88
Total	100.00			

*Calculated by difference to 100 wt%;
[§]Calculated on the basis of 4 P *a.p.f.u.* and charge balance between cationic and anionic population. The resulting structural formula is

$$^{M(1),M(2),M(3)}\left(Mn^{2+}_{3.61}Fe^{2+}_{1.21}Ca_{0.11}Mg_{0.03}\right)_{\Sigma=4.96}\left(^{P(2)}PO_4\right)_2\left(H^{P(1)}_{1.04}PO_4\right)_2(H_2O)_{3.92}$$

mosaicity or fractures, which adversely affect the quality of the diffraction data and, as a consequence, of the structure refinement.

Single-crystal neutron Laue data (crystal size: $1.2 \times 0.9 \times 0.6$ mm^3) were collected at room temperature on the Laue diffractometer KOALA on the OPAL reactor at the Australian Nuclear Science and Technology Organization (ANSTO). KOALA uses the Laue diffraction technique on a non-monochromated thermal neutron beam with a large solid-angle (8 steradian) cylindrical image-plate detector to increase the detected diffracted intensity by one-to-two orders of magnitude compared with a conventional monochromatic experiment (McIntyre *et al.*, 2006). A total of twenty Laue diffraction patterns, each accumulated over 3 h, were collected at 15° intervals in rotation of the hureaulite crystal perpendicular to the incident neutron beam. The crystal was rotated 90° about the incident beam after the first 13 patterns to avoid bias in the final refined anisotropic displacement parameters due to the blind region in reciprocal space around the single instrument rotation axis for one crystal orientation alone. The data extended to a minimum *d* spacing of 0.6 Å. The Laue patterns were indexed using the program LAUEGEN of the Daresbury Laboratory Laue Suite (Campbell, 1995; Campbell *et al.*, 1998), and the reflections integrated using the program INTEGRATE+ (which uses a two-dimensional version of the minimum $\sigma(I)/I$ algorithm, Wilkinson *et al.*, 1988). Correction for absorption was deemed unnecessary in view of the small crystal size. The reflections were normalised for the incident wavelength, using a curve derived by comparing equivalent reflections and multiple observations, and corrected for the different angles of incidence via the local program LAUE4 (Piltz, 2011). Reflections were observed with wavelengths between 0.8 Å and 5.2 Å. In all, 23227 reflections were observed, and yielded 2353 unique reflections in the Laue class 2/*m* (Table 2). The reflection conditions suggested the space group *C*2/*c*.

A low-temperature single-crystal neutron diffraction experiment was performed on a crystal of hureaulite ($3.4 \times 3.1 \times 2.8$ mm^3) using the hot source (fast neutrons) diffractometer HEiDi of the neutron source Heinz Maier-Leibnitz Zentrum (MLZ). The diffraction data were collected at 2.3 K, with a wavelength of the incident beam of 1.1620(2) Å [Ge-311 monochromator, Er foil filter to suppress $\lambda/3$ contamination]. A ^{3}He single-counter detector was used. The sample was fixed on an aluminium pin (0.8 mm diameter) and mounted on a closed-cycle cryostat to reach a minimum temperature of 2.3 K ($\pm$ 0.1 K accuracy). The unit-cell parameters were refined on the basis of 22 Bragg reflections (Table 2), confirming a monoclinic lattice. The unit-cell edges at low temperature are similar to those measured at room temperature, with virtually identical unit-cell volumes. A full set of unique Bragg reflections measured up to $2\theta = 30°$ did not show any violation of the *C*-centred lattice. A total number of 2078 reflections were collected up to $2\theta_{max} = 102.1°$ (with $-21 \leq h \leq 22$, $-11 \leq k \leq 8$ and $-12 \leq l \leq 12$, Table 2) using a pure ω-scan with corresponding vertical beam collimation to avoid cut-off effects (Table 2), out of which 1473 were unique in the Laue class 2/*m* (Table 2). Integrated intensities were then corrected for the Lorentz effect; absorption correction was found to be negligible. The discrepancy factor for the symmetry-related reflections was $R_{int} = 0.0591$ (Table 2). The reflection conditions suggested the space group *C*2/*c*. Further details pertaining to the data collection are reported in Table 2.

3) Mössbauer spectroscopy

Transmission ^{57}Fe Mössbauer spectra were collected at room temperature using a Mössbauer apparatus (HALDER electronics, Germany) in horizontal arrangement (^{57}Co/Rh single-line thin source, constant acceleration mode, symmetric triangular velocity shape, multi-channel analyser with 1024 channels, velocity scale calibrated to α-iron). For the Mössbauer spectroscopy experiment, absorber preparation samples were carefully ground under ethanol, filled into Cu rings (inner diameter 10 mm and covered with a high-purity Al foil on one side), and mixed with epoxy resin to fix the sample. The folded spectra were analysed using classical full static Hamiltonian site analysis (using Lorentzian-shaped doublets).

Table 2. Details of neutron data collections and refinements of hureaulite.

Crystal shape	Prismatic	Prismatic
Crystal size (mm^3)	$1.2 \times 0.9 \times 0.6$	$3.4 \times 3.1 \times 2.8$
Crystal colour	Pale pink	Pale pink
Unit-cell parameters	$a = 17.603(6)$ Å	$a = 17.466(6)$ Å
	$b = 9.087(2)$ Å	$b = 9.104(5)$ Å
	$c = 9.404(4)$ Å	$c = 9.457(4)$ Å
	$\beta = 96.66(4)°$	$\beta = 96.33(6)°$
	$V = 1494.1(9)$ Å^3	$V = 1494.6(12)$ Å^3
Reference formula	$(Mn,Fe)_5(PO_4)_2(HPO_4)_2(H_2O)_4$	$(Mn,Fe)_5(PO_4)_2(HPO_4)_2(H_2O)_4$
Space group	$C2/c$	$C2/c$
Z	4	4
T (K)	293	2.3
Radiation	Polychromatic, neutron	Monochromatic, neutron
Diffractometer	KOALA, Laue diffractometer	HEiDi, 4-circle diffractometer
$\lambda_{min}/\lambda_{max}$ (Å)	0.8/5.2	1.1620
Scan type, steps and width:		
− type	Stationary crystal – stationary detector Laue patterns at 15° intervals around the vertical axis; detector solid angle: +/-144° horizontally, +/-52° vertically	Pure ω-scan; $2\theta < 70°$: 63 steps, 60' vertical collimation; $2\theta > 70°$: 51 steps, 30' collimation
− time per step (s)		2–8
− width; u, v, q		25, 0, 0
d_{min} (Å)	0.6	0.75
	$-26 \leq h \leq 26$	$-21 \leq h \leq 22$
	$-13 \leq k \leq 13$	$-11 \leq k \leq 8$
	$-14 \leq l \leq 14$	$-12 \leq l \leq 12$
No. measured refl.	23227	2078
No. unique refl.	2353	1473
No. uniq. refl. $F_o > 4\sigma(F_o)$	1632	707
No. refined param.	174	167
R_{int}	0.0742	0.0591
$R_1 (F)$, $F_o > 4s(F_o)$	0.0729	0.0747
$R_1 (F)$ all unique refl.	0.1195	0.1289
$wR_2 (F^2)$	0.1237	0.1240
GooF	1.451	1.547
Weigh. scheme: a, b	0.01, 0	0.01, 0
Residuals (fm/Å^3)	$-1.2/+1.4$	$-0.9/+ 1.0$

Notes: $R_{int} = \sum|F_{obs}^2 - F_{obs}^2(mean)|/\sum[F_{obs}^2]$; $R_1 = \sum||F_{obs}| - |F_{calc}||/\sum|F_{obs}|$;
$wR_2 = [\sum[w(F^2_{obs} - F^2_{calc})^2]/\sum[w(F^2_{obs})^2]]^{0.5}$, $w = 1/[\sigma^2(F_{obs}^2) + (aP)^2 + bP]$, $P = (Max (F_{obs}^2, 0) + 2F_{calc}^2)/3$.
For the Laue data: unit-cell parameters based on single-crystal X-ray diffraction data. For the HEiDi data: ω-scan width $= (u + v \cdot \tan\theta + q \cdot \tan2\theta)^{0.5}$.

Results: neutron structure refinement of hureaulite

Two structure refinements of hureaulite were performed on the basis of the intensity data collected at 293 K (Laue data, ANSTO) and at 2.3 K (four-circle diffractometer data, MLZ), respectively.

The neutron intensity data collected at 293 and 2.3 K were first processed to calculate the normalized structure factors (E's) and their statistical distributions using the program E-STATISTICS, as implemented in the WinGX package (Farrugia, 1999). The structure was found to be centrosymmetric (with 94% likelihood at 2.3 K). The structure refinements based on the two data sets were then performed in the space group $C2/c$ using the SHELX-97 software (Sheldrick, 1997, 2008), starting from the (H-free) structure model of Menchetti & Sabelli (1973). The neutron scattering lengths of Fe, Mn, Ca, P, O, and H were used according to Sears (1986). Since the Laue

method does not allow precise estimation of the absolute volume of the unit cell, the refinement at 293 K was conducted with the unit-cell parameters based on single-crystal X-ray diffraction (Table 2). In both neutron refinements, the effects of secondary isotropic extinction were adequately corrected by Larson's formalism (Larson, 1967), as implemented in SHELXL-97. The three independent octahedral sites $M(1)$, $M(2)$ and $M(3)$ were modelled with a mixed (Fe + Mn) scattering length and the fractions of Fe and Mn on each site were refined (Table 3). The two independent tetrahedral sites (*i.e.*, $P(1)$ and $P(2)$, Table 3) were modelled with the scattering length of P. When convergence was achieved, five negative residual peaks were found in the final difference-Fourier map of the nuclear density. The final cycles of anisotropic refinement were then conducted assigning H to these residual peaks (as hydrogen has a negative neutron scattering length; $H(1–5)$ in Table 3). Any attempt to allocate Ca at one of the octahedral sites was unsuccessful, likely due to its low

concentration (Table 1). The refinement based on the (Laue) data collected at 293 K was conducted with *M(2)* modelled isotropically, that at 2.3 K with *M(1)*, *M(2)* and *M(3)* modelled isotropically; all the other atomic sites (H included) were refined anisotropically. Convergence was rapidly achieved, with no significant correlation among the refined parameters in the variance-covariance matrix. At the end of the refinements, no peaks larger than $\pm$ 1.4 $fm/\text{Å}^3$ and $\pm$ 1.0 $fm/\text{Å}^3$ were found in the final difference-Fourier map of the nuclear density at 293 and 2.3 K, respectively (Table 2), and their final agreement indices were $R_1 = 0.0729$ (for 174 refined parameters and 1632 unique reflections with $Fo > 4\sigma(Fo)$) at 293 K, and $R_1 = 0.0747$ (for 167 refined parameters and 707 unique reflections with $Fo > 4\sigma(Fo)$) at 2.3 K (Table 2). Site coordinates and displacement parameters are listed in Table 3, bond lengths and angles in Table 4.
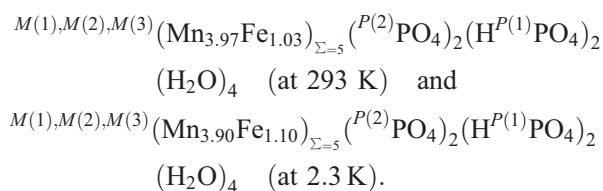
Results: Mössbauer spectrum of hureaulite

The ^{57}Fe Mössbauer spectrum of hureaulite is shown in Fig. 2. It shows four well-separated absorption lines which can be evaluated by two or three doublets for Fe^{2+}; there is no evidence for ferric iron in the sample. While a two-doublet analysis yields acceptable fit, but cannot reproduce a slight asymmetry and exhibits some misfit of the two innermost lines, a three-doublet fit is significantly better (reduced χ^2 of 1.14 as compared to 3.48 for two doublets), and consistent with the findings of Moreira *et al.* (1994) and Bustamente *et al.* (2005). The ^{57}Fe-Mössbauer parameters are listed in Table 5 and are in line with the observations of the literature. All three doublets have similar and, at the same time, small line widths, indicative of well-defined distortion environments around the Fe^{2+} probe nuclei. Following Bustamente *et al.* (2005), the well-resolved doublet with the largest quadrupole splitting is assigned to the *M(3)* site. Assuming an equal distribution of iron, the area fraction of this site should be 40%, but the observed value is distinctly below, suggesting a pronounced preference for Mn^{2+} for the *M(3)* site. The two innermost doublets have almost identical isomer shifts and slightly different quadrupole splitting values. In line with the previous studies, the smaller quadrupole splitting value is assigned to the *M(2)* site, which thus should show slightly lower polyhedral distortions than the *M(1)* site. Indeed this is true for both the quadratic octahedral elongation [*i.e.*, $<\lambda>$; 1.015 at *M(2)* and 1.0201 at *M(1)*] and the quadratic octahedral angle variance [*i.e.*, σ^2, 44.4 for *M(2)* and 68.1 for *M(1)*] (Robinson *et al.*, 1971), as deduced on the basis of the neutron structure refinement (at 293 K) of this study (Table 4). Additional proof for this site assignment comes from relative area fractions, which are in adequate agreement with the ones obtained from neutron diffraction. The distinct overlap of doublets from *M(1)* and *M(2)* site leaves some uncertainties in the exact area fractions for these two sites from Mössbauer spectroscopy, while the relative area fraction on *M(3)* shows excellent
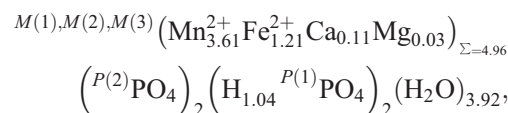
agreement with the results obtained from neutron diffraction.

Discussion

The EPMA-WDS data show that our hureaulite sample has Mn $\gg$ Fe (Table 1); Ca and Mg are only minor substituents for these cations on the octahedral sites. No substituents for P, at the tetrahedral sites, have been found at a significant level. The chemical formula deduced on the basis of the neutron structure refinements at 293 K (*i.e.*, based on Laue data) and at 2.3 K (*i.e.*, based on monochromatic data) are mutually consistent:

$$^{M(1),M(2),M(3)}(Mn_{3.97}Fe_{1.03})_{\Sigma=5}(^{P(2)}PO_4)_2(H^{P(1)}PO_4)_2$$
$$(H_2O)_4 \quad \text{(at 293 K)} \quad \text{and}$$
$$^{M(1),M(2),M(3)}(Mn_{3.90}Fe_{1.10})_{\Sigma=5}(^{P(2)}PO_4)_2(H^{P(1)}PO_4)_2$$
$$(H_2O)_4 \quad \text{(at 2.3 K)}.$$

There is a good agrement between the chemical formula obtained on the basis of structure refinements and that based on the EPMA-WDS data:

$$^{M(1),M(2),M(3)}(Mn_{3.61}^{2+}Fe_{1.21}^{2+}Ca_{0.11}Mg_{0.03})_{\Sigma=4.96}$$
$$(^{P(2)}PO_4)_2(H_{1.04}^{P(1)}PO_4)_2(H_2O)_{3.92},$$

if we consider the calculated number of electrons at the octahedral sites (*i.e.*, $\sum e^-_{(M1+M2+M3)} = 126.0 \ e^-$ on the basis of the structure refinement at 293 K, $\sum e^-_{(M1+M2+M3)} = 124.3 \ e^-$ on the basis of the EPMA-WDS data, with a difference of 1.4%).

The neutron structure refinements of this study confirm the general structure model of hureaulite previously obtained by X-ray diffraction (*e.g.*, Menchetti & Sabelli, 1973; Moore & Araki, 1973). The structure contains $^{P(2)}PO_4$ and (HO $^{P(1)}PO_3$) building units (with two independent tetrahedral sites: *P(1)* and *P(2)*; Tables 3 and 4, Fig. 1) and groups of edge-sharing $^{M(1)}MO_6$, $^{M(3)}MO_5(H_2O)$ and $^{M(2)}MO_4(H_2O)_2$ units (with three independent octahedral sites: *M(1)*, *M(2)* and *M(3)*; Tables 3 and 4, Fig. 1). No "zeolitic" H_2O molecules occur in the hureaulite structure. The two independent P-tetrahedra are slightly distorted, as shown by the mean polyhedral quadratic elongation and by the polyhedral angle variance reported in Table 4. The tetrahedral bond distance *P(1)-O(1)* is longer than the others, and reflects the nature of the *O(1)* as member of the hydroxyl group *O(1)-H(1)* (Table 4). More pronounced are the octahedral distortions (Table 4).

The octahedral site occupancies determined by neutron refinements show that although Mn is dominant at all *M* sites, the highest fraction of Fe occurs at the *M(2)* site ($\sim$36%), with lower fractions observed at *M(1)* and *M(3)* ($\sim$13–15 and $\sim$11–12%, respectively, Table 3). This experimental finding corroborates the conclusion of Moreira *et al.* (1994) and Bustamente *et al.* (2005) on the basis of "indirect" evidence (*i.e.*, polyhedral distortion

Table 3. Site coordinates, occupancy factor (s.o.f.) and anisotropic displacement parameters ($\mathring{A}^2$) of hureaulite based on the structure refinements at 293 K and 2.3 K. The anisotropic displacement factor exponent takes the form: $-2\pi^2[(ha^*)^2 U_{11} +\ldots+ 2hka^*b^* U_{12} + \ldots + 2klb^*c^* U_{23}]$. U_{eq} is defined as one third of the trace of the orthogonalised U_{ij} tensor.

Site	s.o.f.	x	y	z	$U_{iso/eq}$	U_{11}	U_{22}	U_{33}	U_{12}	U_{13}	U_{23}
293 K											
M(1)	Mn 0.869(4), Fe 0.131(4)	0.5	0.6027(7)	0.75	0.013(1)	0.014(2)	0.013(3)	0.013(2)	0	0.003(2)	0
M(2)	Mn 0.645(2), Fe 0.355(2)	0.1898(4)	0.41133(10)	0.3087(7)	0.012(1)*						
M(3)	Mn 0.895(3), Fe 0.105(3)	0.17431(17)	0.02811(43)	0.36438(34)	0.012(1)*						
P(1)	P 1	0.08266(7)	0.17943(18)	0.08977(14)	0.0092(3)	0.0125(4)	0.0070(7)	0.0076(5)	0.0001(5)	0.002(1)	−0.0001(5)
P(2)	P 1	0.33915(8)	0.23885(18)	0.37191(17)	0.0091(3)	0.0116(5)	0.0067(8)	0.0086(6)	−0.0009(5)	−0.0001(4)	−0.0003(5)
O(1)	O 1	0.01178(7)	0.28479(20)	0.08013(15)	0.0169(3)	0.0197(5)	0.0146(8)	0.0154(6)	0.0079(5)	−0.0001(5)	−0.0021(6)
O(2)	O 1	0.07673(7)	0.06661(18)	0.20577(13)	0.0138(3)	0.0188(5)	0.0111(7)	0.0115(5)	−0.0010(5)	−0.0017(5)	0.0036(5)
O(3)	O 1	0.15412(7)	0.27155(19)	0.13394(16)	0.0143(3)	0.0147(5)	0.0148(7)	0.0135(6)	−0.0047(5)	0.0015(4)	−0.0034(6)
O(4)	O 1	0.41560(6)	0.39148(18)	0.05563(13)	0.0138(3)	0.0163(4)	0.0147(7)	0.0101(5)	0.0019(5)	0.0013(4)	−0.0054(5)
O(5)	O 1	0.16365(7)	0.23732(16)	0.46677(13)	0.0117(3)	0.0170(4)	0.0101(7)	0.0081(5)	−0.0001(4)	0.0001(4)	−0.0006(5)
O(6)	O 1	0.29824(6)	0.09561(17)	0.32610(13)	0.0123(3)	0.0151(4)	0.0079(7)	0.0139(5)	−0.0023(5)	0.0016(4)	−0.0016(5)
O(7)	O 1	0.29781(6)	0.36710(17)	0.28986(13)	0.0127(3)	0.0136(4)	0.0103(7)	0.0142(5)	0.0018(5)	0.0016(4)	0.0039(5)
O(8)	O 1	0.42400(7)	0.23415(16)	0.34240(14)	0.0117(3)	0.0118(4)	0.0096(7)	0.0138(5)	0.0001(4)	0.0014(4)	−0.00015(5)
O(9)	O 1	0.26007(7)	0.08052(17)	0.03058(14)	0.0137(3)	0.0180(5)	0.0112(8)	0.0119(5)	0.0008(5)	0.0024(4)	0.0005(6)
O(10)	O 1	0.42233(9)	0.00917(19)	0.15302(20)	0.0214(4)	0.0188(6)	0.0180(10)	0.0279(8)	−0.0027(6)	0.0021(4)	−0.0085(7)
H(1)	H 1	−0.02408(14)	0.27640(35)	−0.01105(29)	0.0266(6)	0.027(1)	0.026(2)	0.026(1)	0.007(1)	0.0051(6)	−0.001(1)
H(2)	H 1	0.29873(14)	0.13063(34)	−0.02110(26)	0.0261(6)	0.033(1)	0.024(2)	0.023(1)	−0.001(1)	−0.001(1)	0.004(1)
H(3)	H 1	0.23782(16)	0.15189(37)	0.08873(29)	0.0310(6)	0.042(1)	0.025(2)	0.028(1)	0.001(1)	0.007(1)	−0.007(1)
H(4)	H 1	0.46576(16)	−0.05140(47)	0.14133(38)	0.0430(8)	0.032(1)	0.045(2)	0.052(2)	0.005(1)	0.013(1)	−0.018(2)
H(5)	H 1	0.43350(16)	0.09080(38)	0.21929(36)	0.0358(7)	0.035(1)	0.026(2)	0.046(2)	−0.006(1)	0.008(1)	−0.014(2)
2.3 K											
M(1)	Mn 0.855(7), Fe 0.145(7)	0.5	0.6041(16)	0.75	0.016(4)						
M(2)	Mn 0.640(6), Fe 0.360(6)	0.1932(12)	0.424(2)	0.313(2)	0.028(6)						
M(3)	Mn 0.883(6), Fe 0.117(6)	0.1740(5)	0.0275(10)	0.3638(8)	0.020(3)						
P(1)	P 1	0.0831(2)	0.1799(4)	0.0896(4)	0.0235(9)	0.025(2)	0.025(2)	0.0196(16)	−0.0041(18)	0.0067(14)	0.0020(14)
P(2)	P 1	0.3390(2)	0.2396(5)	0.3725(4)	0.0229(8)	0.0257(18)	0.023(2)	0.0199(15)	−0.0041(19)	0.0036(13)	0.0016(16)
O(1)	O 1	0.0114(2)	0.2862(4)	0.0803(4)	0.0275(8)	0.0313(19)	0.030(2)	0.0222(14)	0.0003(16)	0.0097(14)	−0.0007(14)
O(2)	O 1	0.0766(2)	0.0677(4)	0.2059(3)	0.0257(8)	0.0311(2)	0.0271(19)	0.0202(14)	−0.0022(17)	0.0060(13)	0.0029(14)
O(3)	O 1	0.1552(2)	0.2730(4)	0.1339(3)	0.0275(8)	0.0320(19)	0.0267(19)	0.0249(15)	−0.0002(18)	0.0080(13)	−0.0014(15)
O(4)	O 1	0.4161(2)	0.3914(4)	0.0568(3)	0.0260(8)	0.0348(19)	0.0226(18)	0.0213(14)	0.0007(17)	0.0065(13)	0.0024(13)
O(5)	O 1	0.16338(18)	0.2385(4)	0.4662(3)	0.0253(8)	0.0265(17)	0.030(2)	0.0208(13)	0.0011(18)	0.0072(12)	−0.0004(13)
O(6)	O 1	0.2978(2)	0.0949(4)	0.3269(3)	0.0249(8)	0.0296(19)	0.024(2)	0.0225(15)	0.0015(16)	0.0071(13)	0.0016(13)
O(7)	O 1	0.2981(2)	0.3665(4)	0.2895(3)	0.0258(8)	0.0277(2)	0.027(2)	0.0244(15)	−0.0002(17)	0.0090(14)	−0.0017(14)
O(8)	O 1	0.42456(18)	0.2330(4)	0.3421(3)	0.0239(7)	0.0297(17)	0.0212(18)	0.0220(13)	−0.0005(16)	0.0081(12)	−0.0042(13)
O(9)	O 1	0.2591(2)	0.0813(4)	0.0301(3)	0.0251(8)	0.0289(19)	0.027(2)	0.0215(16)	−0.0027(18)	0.0102(14)	0.0035(15)
O(10)	O 1	0.4223(2)	0.0101(5)	0.1523(4)	0.0275(8)	0.0317(19)	0.031(2)	0.0202(15)	0.004(2)	0.0063(13)	−0.0037(17)
H(1)	H 1	−0.0241(3)	0.2779(7)	−0.0113(6)	0.0329(14)	0.029(3)	0.039(3)	0.031(3)	0.001(3)	0.004(2)	−0.005(3)
H(2)	H 1	0.2999(4)	0.1292(7)	−0.0215(6)	0.0364(15)	0.040(4)	0.036(4)	0.037(3)	0.002(3)	0.019(3)	0.009(3)
H(3)	H 1	0.2373(4)	0.1518(7)	0.0890(6)	0.0372(15)	0.053(4)	0.028(3)	0.034(3)	0.003(3)	0.019(3)	−0.002(3)
H(4)	H 1	0.4657(4)	−0.0528(8)	0.1424(7)	0.0430(17)	0.039(4)	0.047(4)	0.045(3)	0.009(4)	0.016(3)	−0.013(3)
H(5)	H 1	0.4340(4)	0.0910(8)	0.2200(7)	0.0378(15)	0.043(4)	0.034(4)	0.036(3)	−0.007(3)	0.000(3)	−0.010(3)

*Restrained to the same value.

Table 4. Relevant bond distances (Å) and angles (°) in the hureaulite structure at 293 and 2.3 K.

293 K				2.3 K			
$M(1) - O(2) \times 2$	2.120(5)	$O(2) - M(1) - O(2)$	87.0(3)	$M(1) - O(2) \times 2$	2.129(12)	$O(2) - M(1) - O(2)$	85.5(6)
$M(1) - O(4) \times 2$	2.218(2)	$O(2) - M(1) - O(4)$	103.7(2)	$M(1) - O(4) \times 2$	2.213(4)	$O(2) - M(1) - O(4)$	103.0(4)
$M(1) - O(8) \times 2$	2.239(5)	$O(2) - M(1) - O(4)$	78.3(2)	$M(1) - O(8) \times 2$	2.224(11)	$O(2) - M(1) - O(4)$	78.6(3)
$<M(1) – O>$	2.192	$O(2) - M(1) - O(8)$	168.4(2)	$<M(1) – O>$	2.189	$O(2) - M(1) - O(8)$	168.1(3)
$V_{(M1polyh)}$	13.65	$O(2) - M(1) - O(8)$	88.9(1)	$V_{(M1polyh)}$	13.61	$O(2) - M(1) - O(8)$	90.0(2)
$<\lambda>_{(M1polyh)}$	1.0201	$O(4) - M(1) - O(4)$	177.2(4)	$<\lambda>_{(M1polyh)}$	1.0186	$O(4) - M(1) - O(4)$	177.9(8)
$\sigma^2_{(M1polyh)}$	68.1	$O(4) - M(1) - O(8)$	86.0(2)	$\sigma^2_{(M1polyh)}$	62.5	$O(4) - M(1) - O(8)$	86.8(3)
		$O(4) - M(1) - O(8)$	92.2(2)			$O(4) - M(1) - O(8)$	91.8(3)
$M(2) - O(3)$	2.125(9)	$O(8) - M(1) - O(8)$	97.1(3)	$M(2) - O(3)$	2.22(3)	$O(8) - M(1) - O(8)$	96.4(6)
$M(2) - O(5)$	2.266(9)			$M(2)- O(5)$	2.32(3)		
$M(2) - O(6)$	2.112(9)	$O(3) - M(2) - O(5)$	90.9(4)	$M(2)- O(6)$	2.06(3)	$O(3) - M(2) - O(5)$	87.6(8)
$M(2) - O(7)$	1.974(7)	$O(3) - M(2) - O(6)$	93.0(3)	$M(2)- O(7)$	1.94(3)	$O(3) - M(2) - O(6)$	90.9(8)
$M(2) - O(9)$	2.250(9)	$O(3) - M(2) - O(7)$	90.2(4)	$M(2)- O(9)$	2.16(3)	$O(3) - M(2) - O(7)$	87.3(9)
$M(2) - O(10)$	2.225(8)	$O(3) - M(2) - O(9)$	170.6(4)	$M(2)- O(10)$	2.22(3)	$O(3) - M(2) - O(9)$	172.5(11)
$<M(2) – O>$	2.159	$O(3) - M(2) - O(10)$	100.0(3)	$<M(2) – O>$	2.16	$O(3) - M(2) - O(10)$	97.5(9)
$V_{(M2polyh)}$	13.16	$O(5) - M(2) - O(6)$	171.6(4)	$V_{(M2polyh)}$	13.17	$O(5) - M(2) - O(6)$	171.4(11)
$<\lambda>_{(M2polyh)}$	1.0150	$O(5) - M(2) - O(7)$	100.4(4)	$<\lambda>_{(M2polyh)}$	1.0124	$O(5) - M(2) - O(7)$	99.0(10)
$\sigma^2_{(M2polyh)}$	44.4	$O(5) - M(2) - O(9)$	97.5(3)	$\sigma^2_{(M2polyh)}$	28.9	$O(5) - M(2) - O(9)$	98.6(8)
		$O(5) - M(2) - O(10)$	85.3(3)			$O(5) - M(2) - O(10)$	84.0(8)
$M(3) - O(2)$	2.169(4)	$O(6) - M(2) - O(7)$	87.1(3)	$M(3) - O(2)$	2.167(9)	$O(6) - M(2) - O(7)$	89.4(9)
$M(3) - O(4)$	2.211(4)	$O(6) - M(2) - O(9)$	79.3(4)	$M(3)- O(4)$	2.200(10)	$O(6) - M(2) - O(9)$	83.6(9)
$M(3) - O(5)$	2.149(5)	$O(6) - M(2) - O(10)$	86.7(4)	$M(3)- O(5)$	2.169(10)	$O(6) - M(2) - O(10)$	87.8(9)
$M(3) - O(6)$	2.334(4)	$O(7) - M(2) - O(9)$	84.1(3)	$M(3)- O(6)$	2.311(9)	$O(7) - M(2) - O(9)$	87.7(9)
$M(3) - O(7)$	2.157(4)	$O(7) - M(2) - O(10)$	168.3(5)	$M(3)- O(7)$	2.155(10)	$O(7) - M(2) - O(10)$	174.5(13)
$M(3) - O(9)$	2.269(4)	$O(9) - M(2) - O(10)$	85.0(3)	$M(3)- O(9)$	2.269(9)	$O(9) - M(2) - O(10)$	87.2(8)
$<M(3) – O>$	2.215			$<M(3) – O>$	2.212		
$V_{(M3polyh)}$	13.27	$O(2) - M(3) - O(4)$	77.5(2)	$V_{(M3polyh)}$	13.26	$O(2) - M(3) - O(4)$	78.1(3)
$<\lambda>_{(M3polyh)}$	1.0609	$O(2) - M(3) - O(5)$	93.6(2)	$<\lambda>_{(M3polyh)}$	1.0587	$O(2) - M(3) - O(5)$	93.4(4)
$\sigma^2_{(M3polyh)}$	191.8	$O(2) - M(3) - O(6)$	122.1(2)	$\sigma^2_{(M3polyh)}$	186.9	$O(2) - M(3) - O(6)$	121.9(4)
		$O(2) - M(3) - O(7)$	82.6(2)			$O(2) - M(3) - O(7)$	82.5(4)
$P(1) - O(1)$	1.567(3)	$O(2) - M(3) - O(9)$	162.6(3)	$P(1) - O(1)$	1.579(6)	$O(2) - M(3) - O(9)$	162.8(5)
$P(1) - O(2)$	1.509(3)	$O(4) - M(3) - O(5)$	104.0(2)	$P(1) - O(2)$	1.515(6)	$O(4) - M(3) - O(5)$	104.3(4)
$P(1) - O(3)$	1.528(2)	$O(4) - M(3) - O(6)$	156.8(2)	$P(1) - O(3)$	1.536(6)	$O(4) - M(3) - O(6)$	156.6(5)
$P(1) - O(4)$	1.515(2)	$O(4) - M(3) - O(7)$	94.3(2)	$P(1) - O(4)$	1.531(5)	$O(4) - M(3) - O(7)$	94.0(4)
$<P(1) – O>$	1.530	$O(4) - M(3) - O(9)$	88.1(2)	$<P(1) – O>$	1.540	$O(4) - M(3) - O(9)$	87.5(4)
$V_{(P1polyh)}$	1.83	$O(5) - M(3) - O(6)$	88.2(2)	$V_{(P1polyh)}$	1.87	$O(5) - M(3) - O(6)$	87.7(4)
$<\lambda>_{(P1polyh)}$	1.0013	$O(5) - M(3) - O(7)$	160.1(2)	$<\lambda>_{(P1polyh)}$	1.0018	$O(5) - M(3) - O(7)$	160.1(5)
$\sigma^2_{(P1polyh)}$	4.53	$O(5) - M(3) - O(9)$	99.3(2)	$\sigma^2_{(P1polyh)}$	6.95	$O(5) - M(3) - O(9)$	99.1(4)
		$O(6) - M(3) - O(7)$	77.6(2)			$O(6) - M(3) - O(7)$	78.1(3)
$P(2) - O(5)$	1.539(3)	$O(6) - M(3) - O(9)$	70.2(1)	$P(2) - O(5)$	1.543(5)	$O(6) - M(3) - O(9)$	70.6(3)
$P(2) - O(6)$	1.525(3)	$O(7) - M(3) - O(9)$	89.0(2)	$P(2) - O(6)$	1.540(6)	$O(7) - M(3) - O(9)$	89.4(4)
$P(2) - O(7)$	1.534(3)			$P(2) - O(7)$	1.529(6)		
$P(2) - O(8)$	1.551(2)	$O(1) - P(1) - O(2)$	109.6(2)	$P(2) - O(8)$	1.554(5)	$O(1) - P(1) - O(2)$	109.3(3)
$<P(2) – O>$	1.537	$O(1) - P(1) - O(3)$	107.8(2)	$<P(2) – O>$	1.541	$O(1) - P(1) - O(3)$	107.4(4)
$V_{(P2polyh)}$	1.86	$O(1) - P(1) - O(4)$	107.9(2)	$V_{(P2polyh)}$	1.88	$O(1) - P(1) - O(4)$	107.2(3)
$<\lambda>_{(P2polyh)}$	1.0003	$O(2) - P(1) - O(3)$	107.4(2)	$<\lambda>_{(P2polyh)}$	1.0002	$O(2) - P(1) - O(3)$	107.4(3)
$\sigma^2_{(P2polyh)}$	0.79	$O(2) - P(1) - O(4)$	111.9(2)	$\sigma^2_{(P2polyh)}$	0.52	$O(2) - P(1) - O(4)$	112.3(4)
		$O(3) - P(1) - O(4)$	112.1(2)			$O(3) - P(1) - O(4)$	113.1(4)
		$O(5) - P(2) - O(6)$	109.3(2)			$O(5) - P(2) - O(6)$	108.9(3)
		$O(5) - P(2) - O(7)$	108.7(2)			$O(5) - P(2) - O(7)$	110.4(4)
$O(1)-H(1)$	1.007(3)	$O(5) - P(2) - O(8)$	108.8(2)	$O(1)-H(1)$	1.011(6)	$O(5) - P(2) - O(8)$	108.6(3)
$O(1)-H(1)*$	1.017	$O(6) - P(2) - O(7)$	109.0(2)	$O(1)-H(1)*$	1.019	$O(6) - P(2) - O(7)$	109.0(3)
$O(1)\cdots O(8)$	2.572(2)	$O(6) - P(2) - O(8)$	111.0(2)	$O(1)\cdots O(8)$	2.579(5)	$O(6) - P(2) - O(8)$	110.1(4)
$H(1)\cdots O(8)$	1.566(3)	$O(7) - P(2) - O(8)$	110.0(2)	$H(1)\cdots O(8)$	1.569(6)	$O(7) - P(2) - O(8)$	109.8(3)
$O(1)-H(1)\cdots O(8)$	176.8(3)			$O(1)-H(1)\cdots O(8)$	177.0(6)		
$O(9)-H(2)$	0.992(3)	$O(10)-H(4)$	0.959(4)	$O(9)-H(2)$	1.007(8)	$O(10)-H(4)$	0.963(8)
$O(9)-H(2)*$	1.007	$O(10)-H(4)*$	0.988	$O(9)-H(2)*$	1.020	$O(10)-H(4)*$	0.987
$O(9)\cdots O(3)$	2.650(2)	$O(10)\cdots O(1)$	2.712(2)	$O(9)\cdots O(3)$	2.631(5)	$O(10)\cdots O(1)$	2.696(6)
$H(2)\cdots O(3)$	1.676(3)	$H(4)\cdots O(1)$	1.820(4)	$H(2)\cdots O(3)$	1.650(7)	$H(4)\cdots O(1)$	1.797(8)
$O(9)-H(2)\cdots O(3)$	166.5(3)	$O(10)-H(4)\cdots O(1)$	153.7(3)	$O(9)-H(2)\cdots O(3)$	163.4(6)	$O(10)-H(4)\cdots O(1)$	153.9(7)

Table 4. Continued

293 K				2.3 K			
O(9)-H(3)	0.961(3)	O(10)-H(5)	0.974(4)	O(9)-H(3)	0.956(8)	O(10)-H(5)	0.983(8)
O(9)-H(3)*	0.985	O(10)-H(5)*	0.993	O(9)-H(3)*	0.976	O(10)-H(5)*	0.999
O(9) · · · O(3)	2.803(2)	O(10) · · · O(8)	2.709(2)	O(9) · · · O(3)	2.774(5)	O(10) · · · O(8)	2.708(5)
H(3) · · · O(3)	1.918(3)	H(5) · · · O(8)	1.764(4)	H(3) · · · O(3)	1.894(8)	H(5) · · · O(8)	1.754(8)
O(9)-H(3) · · · O(3)	152.0(3)	O(10)-H(5) · · · O(8)	162.8(3)	O(9)-H(3) · · · O(3)	151.9(6)	O(10)-H(5) · · · O(8)	162.6(7)
H(2)-O(9)-H(3)	108.5(3)	H(4)-O(10)-H(5)	113.9(4)	H(2)-O(9)-H(3)	109.9(6)	H(4)-O(10)-H(5)	113.6(7)

*Bond distance corrected for ''riding motion'' following Busing & Levy (1964).
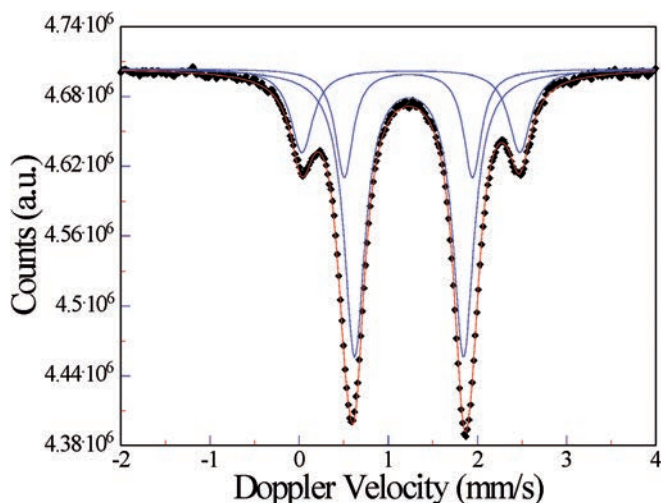
Fig. 2. The ^{57}Fe Mössbauer spectrum of hureaulite at room temperature and the three-doublets fit (reduced χ^2 of 1.14; see text for details). (online version in colour)

deduced on the basis of X-ray structure refinement and Mössbauer spectroscopy), who reported that Mn^{2+} preferentially populates the most distorted M(3) site.

The neutron structure refinements show that five independent H sites occur in hureaulite with full site occupancy (H(1–5), Table 3), one of them as member of the sole hydroxyl group of the structure (O(1)-H(1), Table 4), and the other four belonging to H_2O molecules (H(2)-O(9)-H(3) and H(4)-O(10)-H(5), Table 4). Their displacement parameters are fairly anisotropic (Table 3).

The complex hydrogen bonding scheme in hureaulite structure is now well defined, with five hydrogen bonds energetically favourable (Fig. 3, Table 4). The strongest involves the hydroxyl group, with O(1) as *donor* and O(8) as *acceptor* (i.e., O(1)-H(1) · · · O(8), with H(1) · · · O(8) = 1.566(3) Å at 293 K, Fig. 3, Table 4); the other four bonds involve the H_2O molecules, with O(3) · · · H(2)-O(9)-H(3) · · · O(3) and O(1) · · · H(4)-O(10)-H(5) · · · O(8) (Fig. 3, Table 4). Among the H-bonds of the H_2O molecules, O(9)-H(2) · · · O(3) is stronger than O(9)-H(3) · · · O(3) (with H(2) · · · O(3) = 1.676(3) Å and H(3) · · · O(3) = 1.918(3)

Å at 293 K, Table 4), and O(10)-H(5) · · · O(8) is stronger than O(10)-H(4) · · · O(1) (with H(5) · · · O(8) = 1.764(4) Å and H(4) · · · O(1) = 1.820(4) Å at 293 K, Fig. 3, Table 4). There is, therefore, an asymmetric configuration of the hydrogen-bonding scheme of the two independent H_2O molecules. The H-O-H angles of the two molecules are slightly different: H(2)-O(9)-H(3) = 108.5(3)° and H(4)-O(10)-H(5) = 113.9(4)° (at 293 K, Table 4). The H-bonding scheme described above is retained at low temperature (Table 4).

The present study shows unambiguously that hureaulite contains the $HOPO_3^{2-}$ anion and does not contain H_3O^+, in contrast to the conclusions of Keller (1971).

The neutron structure refinement at 293 K was conducted with the M(2) site modelled isotropically, and the refinement based on the intensity data collected at 2.3 K was conducted with M(1), M(2) and M(3) modelled isotropically. Fully anisotropic refinements gave displacement ellipsoids with unrealistic shapes. An inspection of the difference-Fourier maps of the nuclear density (phased with structural models without the octahedral sites) did not show any evidence, at a significant level, of potential site splitting in order to accommodate different coordination environments (e.g., Fe-Mn or Ca-Mn), which would cause unrealistic displacement parameters if only one site position were considered in the structure refinement. We are inclined to consider that the anomalous shape of the displacement ellipsoids actually reflects problems with the integration of reflection intensities, due to mosaicity and fractures of the crystals.

The ^{57}Fe Mössbauer spectrum of hureaulite confirms the absence of ferric iron in the sample. According to the previous observations of Moreira *et al.* (1994) and Busamente *et al.* (2005), the spectrum shows four well-separated absorption lines which are better fitted with three doublets. The well-resolved doublet (with the largest quadrupole splitting) is here assigned to the M(3) site, in line with the pronounced preference of Mn^{2+} for the M(3) site as obtained by the neutron structure refinements. The two innermost doublets have almost identical isomer shifts, though with slightly different quadrupole splitting values; the smaller quadrupole splitting value is assigned to the M(2) site, which is expected to have a slightly lower

Table 5. ^{57}Fe Mössbauer parameters of hureaulite.

IS (mm/s)	QS (mm/s)	HWHM (mm/s)	Area (%)	Site assignment
1.253(3)	2.445(3)	0.151(4)	19.1(2)	$Fe^{2+}(M(3))$
1.226(3)	1.439(9)	0.127(6)	19.8(9)	$Fe^{2+}(M(1))$
1.233(3)	1.222(8)	0.131(6)	61.1(9)	$Fe^{2+}(M(2))$

Notes: IS = isomer shift, QS = quadrupole splitting with respect to α-iron at room temperature, HWHM = half width at half maximum.
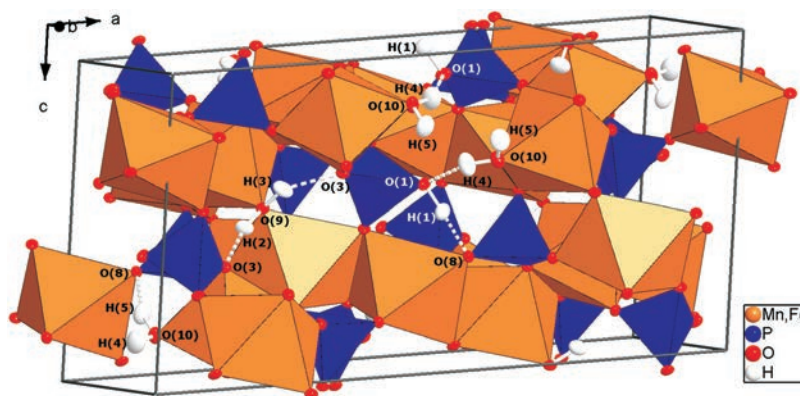

Fig. 3. Clinographic view of the crystal structure of hureaulite with the hydrogen-bonding scheme based on the neutron structure refinement (at 293 K) of this study. Displacement ellipsoid probability factor: 50%. (online version in colour)

polyhedral distortion than the *M(1)* site, according to the experimental findings based on the neutron refinements.

References

Alluaud, F. (1826): Notices sur l'hétérosite, l'hureaulite (fer et manganèse phosphatés), et sur quelques autres minéraux du département de la Haute-Vienne. *Annales des Sciences naturelles*, **8**, 334–354.

Baijot, M., Hatert, F., Dal Bo, F., Philippo, S. (2014): Mineralogy and petrography of phosphates mineral associations from the Jocão pegmatite, Minas Gerais, Brazil. *Can. Mineral.*, **52**, 373–397.

Busing, W.R. & Levy, H.A. (1964): The effect of thermal motion on the estimation of bond lengths from diffraction measurements. *Acta Crystallogr.*, **17**, 142–146.

Bustamante, A., Mattievich, E., de Amoim, H.S., Vencato, I., Silviera, M.M. (2005): The Mössbauer spectrum of synthetic hureaulite: $Fe_5^{2+}(H_2O)_4(PO_4H)_2(PO_4)_2$. *Hyperfine Inter.*, **166**, 599–603.

Campbell, J.W. (1995): LAUEGEN, an X-windows-based program for the processing of Laue diffraction data. *J. Appl. Crystallogr.*, **28**, 228–236.

Campbell, J.W., Hao, Q., Harding, M.M., Nguti, N.D., Wilkinson, C. (1998): LAUEGEN version 6.0 and INTLDM. *J. Appl. Crystallogr.*, **31**, 496–502.

Černý, P. & Ercit, T.S. (2005): The classification of granitic pegmatites revisited. *Can. Mineral.*, **43**, 2005–2026.

Chukanov, N.V, Scholz, R., Zubkova, N.V., Pekov, I.V, Belakovskiy, D.I., Van, K.V., Lagoeiro, L., Graça, L.M., Krambrock, K., de Oliveira, L.C.A, Menezes Filho, L.A.D., Chaves, L.M.S.C., Pushcharovsky, D.Y. (2014): Correianevesite, $Fe^{2+}Mn_2^{2+}(PO_4)_2 \cdot 3H_2O$, a new reddingite-group mineral from the Cigana mine, Conselheiro Pena, Minas Gerais, Brazil. *Am. Mineral.*, **99**, 811–816.

Dyar, M.D., Jawin, E.R., Breves, E., Marchand, G., Nelms, M., Lane, M.D., Mertzman, S.A., Bish, D.L., and Bishop, J.L. (2014): Mössbauer parameters of iron in phosphate minerals: Implications for interpretation of martian data. *Am. Mineral.*, **99**, 914–942.

Farrugia, L.J. (1999): WinGX suite for small-molecule single-crystal crystallography. *J. Appl. Crystallogr.*, **32**, 837–838.

Fisher, J. (1964): Lithian hureaulite from the Black Hills. *Am. Mineral.*, **49**, 398–406.

Fransolet, A.-M. (1976): L'huréaulite: ses propriétés minéralogiques et son rôle dans l'évolution génétique des phases Li(Fe,Mn)PO$_4$. *Bull. Soc. Fr. Minéral. Cristallogr.*, **99**, 261–273.

Frost, R.L. & Erickson, K.L. (2005): Near-infrared spectroscopic study of selected hydrated hydroxylated phosphates. *Spectroch. Acta Part a - Molecular and Biomolecular Spectroscopy*, **61**, 45–50.

Gatta, G.D., Nénert, G., Vignola, P. (2013a): Coexisting hydroxyl groups and H_2O molecules in minerals: A single-crystal neutron diffraction study of eosphorite, $MnAlPO_4(OH)_2 \cdot H_2O$. *Am. Mineral*, **98**, 1297–1301.

Gatta, G.D., Vignola, P., Meven, M., Rinaldi, R. (2013b): Neutron diffraction in gemology: Single-crystal diffraction study of brazilianite, $NaAl_3(PO_4)_2(OH)_4$. *Am. Mineral.*, **98**, 1624–1630.

Gatta, G.D., Jacobsen, S.D., Vignola, P., McIntyre, G.J., Guastella, G., Abate, L.F. (2014a): Single-crystal neutron diffraction and Raman spectroscopic study of hydroxylherderite, $CaBePO_4(OH,F)$. *Mineral. Mag.*, **78**, 723–737.

Gatta, G.D., Vignola, P., Meven, M. (2014b): On the complex H-bonding network in paravauxite, $Fe^{2+}Al_2(PO_4)_2(OH)_2 \cdot 8H_2O$: A single-crystal neutron diffraction study. *Mineral. Mag.*, **78**, 841–850.

Gerault, Y., A. Riou, and Y. Cudennec (1987): Phosphate hydrogenphosphate hydrate de manganese. *Acta Crystallogr.*, **C43**, 1829–1830.

Huminicki, D.M.C. & Hawthorne, F.C. (2002): The crystal chemistry of phosphate minerals. *in* ''Phosphates'', M.L. Kohn, J. Rakovan, and J.M. Hughes, eds. **48**, Reviews in Mineralogy and Geochemistry, Mineralogical Society of America, Chantilly, Virginia, 123–253.

Keller, P. (1971): Die Kristallchemie der Phosphat- und Arsenatminerale unter besonderer Berücksichtigung der Kationen-Koordinationspolyeder und des Kristallwassers. Teil I: Die Anionen der Phosphat- und Arsenat-minerale. *N. Jb. Mineral. Mh.*, **1971**, 491–510.

Larson, A.C. (1967): Inclusion of secondary extinction in least-squares calculations. *Acta Crystallogr.*, **23**, 664–665.

McIntyre, G.J., Lemée-Cailleau, M.-H., Wilkinson, C. (2006): High-Speed Neutron Laue Diffraction Comes of Age. *Physica B*, **385–386**, 1055–1058.

Menchetti, S. & Sabelli, (1973): The crystal structure of hureaulite, $Mn_5(HPO_4)_2(PO_4)_2(H_2O)_4$. *Acta Crystallogr.*, **B29**, 2541–2548.

Moore, P.B. & Araki, (1973): Hureaulite, $Mn_5^{2+}(H_2O)_4[PO_3(OH)]_2[PO_4]_2$: Its atomic arrangement. *Am. Mineral.*, **58**, 302–307.

Moreira, L.F., Domingues, P.H., and Mattievich, E. (1994): Mössbauer studies of the solid solutions of synthetic hureaulite, $[Fe_xMn_{5-x}][PO_4H]_2[PO_4]_2[H_2O]_4$. *J. Magn. Magn. Mater.*, **132**, 191–196.

Pedrosa-Soares, A.C., Chaves, M., Scholz, R. (2009): Eastern Brazilian pegmatite province. *4th International Symposium on Granitic Pegmatites, Field trip guide*, 1–28.

Piltz, R.O. (2011): Accurate data analysis for the Koala and VIVALDI neutron Laue diffractometers. Proceedings of the XXII IUCr Congress, Madrid (Spain), 22–30 August 2011. *Acta Crystallogr.*, **A67**, C155.

Robinson, K., Gibbs, G.V., and Ribbe, P.H. (1971) Quadratic Elongation: A Quantitative Measure of Distortion in Coordination Polyhedra. *Science*, **172**, 567–570.

Sears, V.F. (1986): Neutron scattering lengths and cross-sections. *in* ''Neutron scattering, methods of experimental physics'', K. Sköld and D.L. Price, eds. Vol. 23A, Academic Press, New York, 521–550.

Sheldrick, G.M. (1997): SHELX-97. Programs for crystal structure determination and refinement. University of Göttingen, Germany.

Sheldrick, G.M. (2008): A short history of *SHELX*. *Acta Crystallogr.*, **A64**, 112–122.

Simmons, W., Webber, K.L., Falster, A.U., Nizamoff, J.W. (2003): Pegmatology – pegmatite mineralogy, petrology and petrogenesis. Rubellite Press, New Orleans, Louisiana, 176 p.

Vauquelin, L.N. (1825): Analyse de l'hureaulite, minéral trouvé dans la commune d'Hureaux. *Annales de Chimie et de Physique*, **30**, 302–307.

Vignola, P., Gatta, G.D., Hatert, F., Guastoni, A., Bersani, D. (2014): On the crystal-chemistry of a near end-member triplite, $Mn^{2+}_2(PO_4)F$, from Codera valley (Sondrio Province, Central Alps, Italy). *Can. Mineral.*, **52**, 235–245.

Wilkinson, C., Khamis, H.W., Stansfield, R.F.D., McIntyre, G.J. (1988): Integration of single-crystal reflections using area multidetectors. *J. Appl. Crystallogr.*, **21**, 471–478.